Journal of the Brazilian Society of Mechanical Sciences and Engineering (2020) 42:277
https://doi.org/10.1007/s40430-020-02365-8

TECHNICAL PAPER

Primary atomization of a turbulent liquid jet in crossflow: a comparison between VOF and FGVT methods

Bernardo Alan de Freitas Duarte[1] · Franco Barbi[1] · Millena Martins Villar[1] · Ricardo Serfaty[2] · Aristeu da Silveira Neto[1]

Received: 19 December 2019 / Accepted: 19 April 2020 / Published online: 7 May 2020

Abstract
The primary atomization of a turbulent liquid jet in crossflow was investigated using a mathematical, numerical and computational model. A comparison between the standard volume of fluid (VOF) method and the fine grid volume tracking (FGVT) method was reported. The FGVT method advects the interface between two fluids using a finer grid than the employed by the standard VOF method, and according to the literature, it provides a better interface resolution. Simulations were performed using adaptive mesh refinement in a three-dimensional domain subjected to gravitational field using the in-house code MFSim. The flow was modeled using an Eulerian–Lagrangian approach to capture the interface. The interface was tracked initially with VOF or FGVT methods until the initial breakup. Broken off, small-scale nearly spherical drops were transferred into the Lagrangian point particle description. Column breakup and shear breakup modes were observed on the liquid jet. Drops were small as one-hundredth the size of the injector diameter. The model was validated against experimental correlations for the liquid jet column trajectory, and the droplet size distribution was compared to a previous numerical study from the literature. In addition, the breakup mechanisms predicted were qualitatively compared to those in previous reports. The results of the liquid column trajectory from the simulations performed presented low differences with the literature for both methods tested. According to the numerical results obtained from the computational simulations, the liquid column trajectory was well captured and the droplet size distribution was similar to the literature; however, the FGVT method provided higher accuracy compared to VOF method. The two main breakup modes were identified, namely the column breakup with Kelvin–Helmholtz instabilities and the surface breakup with the formation of multiple ligaments which later lead to droplet formation. The FGVT method provided a more detailed interface contour and improved the number of droplets converted from the Eulerian to the Lagrangian approach compared to the standard VOF method. On the other hand, the FGVT method presented relatively higher computational costs compared to VOF. Therefore, the FGVT method presented a higher interface quality and allowed a larger number of droplet conversion to the Lagrangian approach compared to the VOF method, even though the simulation run time using VOF was lower than with FGVT.

Keywords Lagrangian point particles · Droplet size distribution · Adaptive mesh refinement · Two-phase flows · Kelvin–Helmholtz instabilities

1 Introduction

A complex and important two-phase flow problem of liquid jets in crossflow (JICF) has been modeled using two different numerical methods, namely the conventional VOF method [1] and the fine grid volume tracking (FGVT) method [2]. The FGVT method has been implemented in an in-house code named MFSim and it brought new observations into JICF community. The goal of the present work is to present the potential characteristics of the FGVT method in comparison with VOF method for a fluid dynamic problem

Technical Editor: Erick de Moraes Franklin.

✉ Bernardo Alan de Freitas Duarte
be1988aqua@gmail.com

[1] Federal University of Uberlândia, 2121 Av. João Naves de Ávila, Uberlândia, Brazil

[2] CENPES, Av. 1, Ilha do Fundão, Brazil

where interface resolution is essential to liquid breakup and spray formation.

An investigation of a turbulent liquid jet in crossflow using the computational fluid dynamics (CFD) methodology is reported in the present paper. The interface between the two fluids was modeled using a hybrid Eulerian–Lagrangian approach, where Eulerian droplets may be converted into point particles in order to reduce the mesh computational costs. In addition, the conventional volume of fluid (VOF) method [1] was compared to an improved method previously presented in the literature, where the VOF method was modified in order to obtain higher advection accuracy, namely the fine grid volume tracking (FGVT) method [2]. The FGVT method was previously introduced by Rudman [2], and in the present paper, it was tested for the important engineering application of a turbulent liquid jet breakup. The main goal of the present paper is to perform a benchmark between the VOF and FGVT methods in a liquid jet breakup case with primary atomization using adaptive mesh refinement (AMR). In order to compare the numerical methods, the breakup modes, the liquid jet trajectory and the droplet size distributions were qualitatively compared. The paper was organized in five sections, namely: Sect. 1 (literature review about the theme); Sect. 2 (mathematical and numerical model); Sect. 3 (model validation and results); Sect. 4 (conclusions obtained) and acknowledgments.

1.1 Liquid breakup and spray formation

According to Movaghar et al. [3], the primary breakup may be defined as the process where any liquid surface becomes unstable and droplets are formed. When these drops move according to flow, a spray is formed and characterized [4]. The study of a liquid breakup and its spray may provide relevant information for some practical purposes as well as for fundamental scientific research because understanding liquid breakup and its spray is of high interest to further improve several engineering devices [5]. In the field of combustion, for example, most concepts for current and future high efficiency, and low-emission internal combustion engines employ direct injection of fuel using sprays [3].

Atomization process is severely important, but also quite challenging [6]. The breakup of liquid jets in crossflow (JICF) is considered a complex multiscale phenomenon playing a relevant role in several applications [7]. Atomizing liquid jets are frequently occurring in a number of industrial applications. According to Grosshans [8], due to its importance, these flows have been analyzed extensively by means of experiments in the last decades. However, there is a lack of relevant information related to the breakup mechanisms and spray formation. For example, the influence of fluid properties on the liquid jet breakup is yet few understood [8]. In addition, the detailed structure within the main spray region is not yet fully understood [9]. According to [3], the limited understanding of primary breakup is due to the fact that experimental observation of the high-density region close to jet inlet may be considered extremely difficult. As a result, the underlying physics leading to primary breakup is still not clarified. According to Bravo [10], a full understanding of the primary atomization process has not been achieved for several reasons, including difficulties in visualizing the main dense region. According to Grosshans et al. [8], due to the large number of droplets, experimental measurements in these flow regions may be very challenging. Regarding droplet size distributions in dense sprays, results are mainly blurred. On the other hand, in computational simulations, it is difficult to model the primary breakup phenomena due to the interface resolution requirement, since it demands great computational costs, especially for high Weber and Reynolds numbers [5]. According to Bravo et al. [10], the performance of simulations with high grid resolution to study turbulent atomizing flows has become an interesting alternative complementing material experiments with the advances in computing power and numerical algorithms.

According to Denner et al. [11], the VOF method naturally captures and represents interface breakup and coalescence without any other additional models, although very fine meshes may be required. On the other hand, if the mesh quality is low, some inaccurate results may be obtained [5]. Due to the advances in numerical methods and computing resources in the last decades, CFD simulations with high resolution of atomizing flows are now more commons than before, providing new insights into the literature [10].

It is known that liquid jets with transverse injection provide high atomization efficiency and droplet generation due to the enhanced interaction of aerodynamic shear forces between the liquid jet and the crossflows [7]. Since it enhances turbulence, it has several applications for mixing in engineering. Nowadays, CFD is widely employed in liquid jets with transverse injection and more recently coupled with phase change models, as seen in Duarte et al. [12] and Lee et al. [13].

According to Grosshans [8], the main characteristics of a primary breakup of a fuel jet is the breakup length and droplet diameter, since it is important to combustion processes efficiency. The amount and sizes of droplets in liquid-fueled systems are crucial parameters related to the performance characteristics in engines [7] since the characteristics of the multiple droplets significantly modify these environments [9]. In addition, liquid spray penetration is a very relevant parameter in engineering applications related to JICF because it is often used to indicate the potential for efficient fuel–air mixing [14].

In the present work, adaptive mesh refinement (AMR) was used in the computational simulations, where mesh is adapted to the flow dynamically according to the presence of

the interface. Simulations using uniform grids increase the computational costs due to the refinement of all the domains. Previous works have demonstrated a relevant reduction in computational power requirement when using AMR compared to uniform grids [15]. Duarte et al. [16] presented the increase of almost 50% in computational efficiency using AMR in several two-phase flows problems. AMR is particularly relevant in cases where only a small region of the computational domain should be solved using a fine grid, which is the case of spray breakup where a large flume is usually used as domain. AMR is an important tool for the case investigated in the present paper since more than 70% of the computational domains consist of a region where there is no interface between fluids. Finally, AMR reduces the computational costs of the simulations without affecting numerical accuracy with a high efficiency [16].

1.2 Turbulence in JICF

Kelvin-Helmholtz instability is commonly seen in JICF due to the occurrence of shear between the interface of the two fluids, as previously reported by Herrmann [17] and Grosshans et al. [8]. The Kelvin–Helmholtz instability naturally occurs when two layers of fluids move with different speed lying close to each other. Therefore, the primary cause of Kelvin–Helmholtz instability is the vorticity magnitude in a parallel shear layer and evidences of Kelvin–Helmholtz instability may be confirmed by q-criterion iso-surfaces. A value of q-criterion is mathematically given by a positive value of the second invariant from the velocity gradient tensor. The velocity gradient tensor (A) is a second order tensor and it can be decomposed into two parts (symmetric and anti-symmetric):

$$A_{ij} = S_{ij} + \Omega_{ij}, \tag{1}$$

where S_{ij} is known as rate-of-strain tensor, given by:

$$S_{ij} = \frac{1}{2}\left(\frac{\partial u_i}{\partial x_j} + \frac{\partial u_j}{\partial x_i}\right), \tag{2}$$

and Ω_{ij} is known as the vorticity tensor, given by:

$$\Omega_{ij} = \frac{1}{2}\left(\frac{\partial u_i}{\partial x_j} - \frac{\partial u_j}{\partial x_i}\right), \tag{3}$$

where the vorticity represents twice the angular velocity (ω) [18] and it can be mathematically defined as:

$$\Omega = 2\frac{\mathrm{d}\omega}{\mathrm{d}t}. \tag{4}$$

Since the second invariant (named here as B) from the tensor A can be decomposed into a symmetric and anti-symmetric part, then it can be seen that the q-criterion is a local balance between the shear strain rate S_{ij} and the vorticity magnitude Ω_{ij} according to the following expression:

$$B = \frac{1}{2}\left(\mathrm{tr}(A)^2 - \mathrm{tr}^2(A)\right) = \frac{1}{2}\left(\|\Omega\|^2 - \|S\|^2\right), \tag{5}$$

where tr represents the trace of the tensor (summing the diagonals of the matrix of components).

Since the q-criterion is defined by the second invariant (B) from the velocity gradient tensor (A), it can be understood as a positive balance between the vorticity magnitude Ω_{ij} and the shear strain rate S_{ij}, defining surfaces where vorticity magnitude is greater than rate-of-strain magnitude [19]. Therefore, a surface with a given q-criterion value basically represents a balance between the local shear strain rate and the angular velocity, where necessarily the vorticity is higher than the strain rate since q-criterion is always positive.

1.3 Eulerian–Lagrangian interface capturing model

The Eulerian–Lagrangian interface capture method is a hybrid approach to reduce the computational costs associated with the Eulerian description of a high number of dispersed phase entities in the computational domain. According to Movaghar et al. [3], Eulerian–Lagrangian models are the current platforms for engineering simulations of spray processes for even fuel injection in engines. Since a Lagrangian droplet does not require a fine grid to be represented, an Eulerian–Lagrangian approach is very relevant to a simulation with liquid breakup where a large domain portion is occupied by droplets.

Engineering processes related to atomization typically produce a large number of drops with multiple sizes, and when a vast number of drops are formed, the complexity of tracking all the interfaces becomes a challenging task even using CFD. Tracking multiple interfaces in CFD simulations, especially when there is a large number of droplets may become even prohibitive since the computational costs might be excessively high [17]. In order to reduce the costs of tracking multiple interfaces in CFD problems, a Lagrangian approach may be introduced in which the drop is treated as a point particle, not requiring an Eulerian mesh resolution to solve its representation. This alternative approach assumes that droplets smaller than a certain cutoff length scale are converted in a point particle. The criterion for a drop transfer from the Eulerian to the Lagrangian approach is based on two prerequisites [17]:

- $V_{\mathrm{drop}} < V_{\mathrm{criterion}}$,
- $r_{\max} < 2\left(\frac{3}{4\pi}V_{\mathrm{drop}}\right)$.

Therefore, the drop transfer occurs when a separated liquid structure has a liquid volume (V_{drop}) smaller than a previous

criterion ($V_{\text{criterion}}$) and its shape must be nearly spherical. (The maximum radius would be twice as expected for a perfect sphere.) The second criterion is severely relevant to cases where flow is subjected to shear since it allows the detached ligament structures continue to break up.

1.4 Fine grid volume tracking (FGVT) method

The fine grid volume tracking (FGVT) method was employed in the simulations in order to capture the interface more accurately than using the standard VOF method. The VOF method was developed by Hirt and Nichols [1] and later improved by the PLIC algorithm by Wachem et al. [20]. On the other hand, in the FGVT method, the interface between the two fluids is advected on a computational grid that is twice as fine as the one used for linear momentum and pressure. The FGVT numerical method employed in this investigation was previously presented and tested by Rudman [2].

The FGVT method consists of employing two grids in the computational simulations: the standard and the fine grid, namely the $N \times N \times N$ grid used for momentum and pressure solution (standard grid) and the one used for VOF advection (fine grid). According to Rudman [2], the use of a finer grid in the interface advection (FGVT) provided in all the simulations tested smaller errors compared to the advection at standard grids (VOF).

Figure 1 shows an schematic figure illustrating the standard grid (dx, dy) with VOF and the fine grid used by FGVT (dx/2, dy/2) here considering only a two-dimensional analysis.

As shown in Fig. 1, more details about the interface shape and position are possible when using the finer grid with the FGVT method. According to Fig. 1, the VOF advection is executed in a finer grid than the solution of the pressure and velocities fields; therefore, the time step employed in the simulation must be reduced by a factor of two in order to capture the interface position without reducing accuracy.

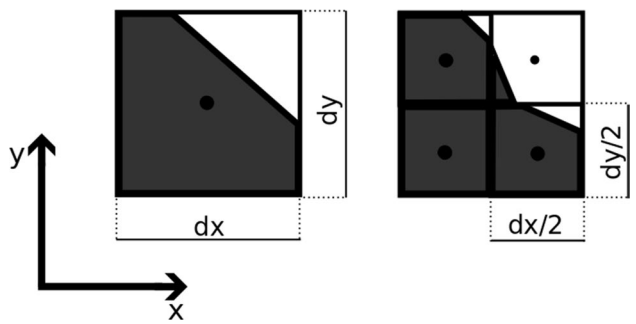

Fig. 1 Schematic bidimensional illustration of the grid employed when using the VOF (left) and FGVT (right) methods. The volume fraction (shadow in gray) details are better captured in the fine grid (dx/2, dy/2) with FGVT compared to the standard (dx, dy) grid with VOF

2 Methodology

2.1 Mathematical model

Considering low Mach number and flow without temperature variations, the continuity equation is expressed according to the following equation:

$$\nabla.\mathbf{v} = 0, \tag{6}$$

where $\mathbf{v}$ is the velocity. The divergence-free conditions may be expected since the temperature variations may be neglected in the simulations performed.

The linear momentum balance equation is given by the following expression:

$$\rho\left(\frac{\partial \mathbf{v}}{\partial t} + \nabla.(\mathbf{vv})\right) = -\nabla p + \nabla.\left[\mu\left(\nabla\mathbf{v} + (\nabla\mathbf{v})^T\right)\right] + \rho\mathbf{g} + \mathbf{f}_{\text{st}}, \tag{7}$$

where p is the pressure, ρ is the specific mass, μ is the dynamic viscosity, $\mathbf{g}$ is the gravity field and $\mathbf{f}_{\text{st}}$ is a source term to take into account the effects of surface tension.

The effects of surface tension are included in the formulation using the model of Brackbill et al. [21]. This model specifies the surface tension force per unit volume according to the expression:

$$\mathbf{f}_{\text{st}} = \frac{\rho\sigma\kappa\nabla\alpha}{\frac{1}{2}(\rho_l - \rho_v)}, \tag{8}$$

where σ is the surface tension coefficient, κ is the local curvature and α is the volume fraction of the dispersed phase.

2.2 MFSim code

The partial differential equations were solved with a standard finite volume method on a staggered rectangular three-dimensional grid. The velocity–pressure coupling was accomplished using a two-step projection method [22] with an explicit treatment for advection terms and an implicit treatment for pressure and diffusion terms. The Barton scheme [23] was used for the spatial discretization of the advective terms. The transient equations were solved using a finite volume methodology.

The transient equations were solved using the MFSim program, which has been developed over the last ten years in cooperation with a large research group and with the scientific support of Petrobras, a semipublic Brazilian multinational corporation in the petroleum industry, headquartered in Rio

de Janeiro, Brazil. For further details about the code and its previous works, the readers are invited to see [12, 16, 24].

All simulations were performed in a parallel environment in the fluid mechanics laboratory cluster at the Federal University of Uberlândia, Brazil. The code uses single-block and multi-block structured meshes and a variable time step. The magnitude of the allowable time step for stable calculations is determined from the advective and diffuse terms. The constraint is defined according to the CFL (Courant–Friedrichs–Lewy) condition and the mesh size [25].

The tolerance of the numerical model in providing a solution to the continuity and linear momentum equations was defined according to the following expression:

$$\text{tol} = \min\left(0.5 \times \delta s^2, 1 \times 10^{-6}\right), \tag{9}$$

where δs is the dimension of the computational cell with the highest resolution in the computational domain. The tolerance expression shown is commonly applied in CFD, specially in two-phase flows. In order to ensure the incompressibility condition, the velocity divergence in each computational cell was evaluated and was not higher than 10^{-11} s^{-1} during all the performed simulations.

2.3 Interface capturing method

The VOF method [1] and the FGVT method [2] were employed to determine the location of interface and its transport with PLIC [20]. The difference between the standard VOF and FGVT methods is only the advection step, since the advection in FGVT method occurs in a grid with higher resolution than the grid employed by the solvers and by the standard VOF advection. The algorithm of the FGVT method was introduced in the MFSim code based on the work of Rudman [2] and using the previous standard VOF method in the MFSim code. The code user can then define whether the standard VOF or FGVT method will be applied to the interface advection in a two-phase flow simulation.

The VOF method (standard and FGVT) employs a color function $\varphi(\mathbf{x}, t)$ to indicate the fractional amount of fluid present at a certain position $\mathbf{x}$ and at time t. The color function φ is calculated using the following equation [20]:

$$\frac{\partial \varphi}{\partial t} + [\mathbf{v}_{\text{normal}}.\nabla\varphi] = 0. \tag{10}$$

The flow fluid properties were calculated based on the volume fraction of the continuous and dispersed phases, as Deen et al. [26]:

$$\rho = \varphi\rho_{\text{dis}} + (1-\varphi)\rho_{\text{con}}, \tag{11}$$

$$\mu = \varphi\mu_{\text{dis}} + (1-\varphi)\mu_{\text{con}}. \tag{12}$$

The VOF (standard and FGVT) method applied in the MFSim code employed the PLIC algorithm [20] and the curvature was computed using the least squares method [11]. The PLIC method is characterized by the construction of a plane which is located geometrically within the dual volume and oriented in the direction of the local surface normal. The PLIC method can easily construct a monotone advection scheme while conserving mass because the mass flux can be calculated geometrically from the planar approximation of the phase interface. The key point in the PLIC method is the reconstructed plane segment in each cell, determined by the normal vector to the interface and its occupied volume within a cell [10]. The conventional VOF model was previously validated in Barbi et al. [27], where spurious currents were evaluated for even multiple bubbles.

The whole domain formulation treats the interface as diffuse, using the delta function method (delta). The earliest two-phase works used the delta method, described in Duarte et al. [16]. Using the diffuse approach, the jump conditions at the interface are expressed by introducing singular source terms in the equations.

$$\mathbf{v}^* = \mathbf{v}^n - \Delta t\left[\mathbf{v}^n.\nabla\mathbf{v}^n - \frac{\nabla.(2\mu D^n)}{\rho^{n+1}} + \frac{\sigma\kappa\mathbf{n}}{\rho^{n+1}} - \mathbf{g}\right], \tag{13}$$

$$\nabla.\left(\frac{\nabla p^{n+1}}{\rho^{n+1}}\right) = \frac{\nabla.\mathbf{v}^*}{\Delta t}, \tag{14}$$

$$\mathbf{v}^{n+1} = \mathbf{v}^* - \Delta t\frac{\nabla p^{n+1}}{\rho^{n+1}}. \tag{15}$$

where D is the deformation rate tensor [18].

2.4 Eulerian–Lagrangian interface capturing algorithm

The conversion of Eulerian droplets to the Lagrangian framework is introduced in the code using an algorithm that identifies individual liquid droplets. The algorithm starts searching for a cell considering VOF color function value greater than zero. When a liquid cell is identified, a search based on breadth-first search (BFS) algorithms is performed to gather the indexes which belong to each given structure; then, the data are kept on a list. Droplet's characteristics are calculated as the search proceeds, and cells that are visited are marked on a logical array. If the structure volume is greater than the conversion volume criteria, the calculation of characteristics are canceled and the list of indexes are cleaned. At this point, the search continues at the same structure to mark its cells as visited. If the structure's calculated volume is smaller than the conversion volume criteria, the indexes are stored with droplet's information, such

as centroid position and diameter. The search process ends when all the cells marked, and all Eulerian droplets are converted by changing the volume fractions of each cell stored by its index and a Lagrangian droplet is added. Each Lagrangian droplet is introduced in the computational domain with its respective diameter at the location of the centroid calculated in the Eulerian framework.

On parallel applications of distributed memory, the search algorithm also stores the ghost cells located in other processors, even for structures that are larger than the volume criteria. This is required in order to notify neighbor processes in which those cells are part of a structure with volume greater than criteria and it avoids the conversion of small parts of the structure that remains in other processes. For liquid structures that are locally smaller than the volume criteria, the ghosts cells located in other processes are necessary to establish the connection between structures that crosses processes limits, so calculations of centroids and diameters are performed correctly. Finally, after the Lagrangian particle is added, its initial velocity is interpolated from the Eulerian field.

2.5 Turbulence model

According to Movaghar et al. [3], direct numerical simulations (DNS) and high-resolution large eddy simulations (LES) are suitable approaches to study liquid–gas interface dynamics during primary breakup. LES is based on the Kolmogorov hypothesis in which the large-scale structures are dependent on the specific flow situation, while the behavior of the small-scale structures is isotropic and geometry independent. Therefore, by using LES, the large-scale structures are captured, while the small-scale structures are filtered out. When applying any spatial filtering to the Navier–Stokes equations, new terms appear, which may be called sub-grid-scale (SGS) terms. Hence, when the scales filtered are small enough to be considered as isotropic, the SGS terms can be closed by a turbulence model. A large number of models have been formulated in the past out of which many are based on the simple Smagorinsky model [8].

Therefore, sprays may be well represented and modeled using LES, as previously reported by Herrmann [17] and Grosshans et al. [8]. In the present work, turbulence was modeled using LES and the turbulence closure was done via the Smagorinsky model with constant of 0.1.

2.6 Case setup

The computational domain consisted of a channel with square section of 0.04 m and it was 0.1 m long. The injector presented a circular section with a diameter of 1.3 mm. The mesh employed consisted of seven levels and the AMR criterion was the presence and proximity of the interface. The mesh resolution of the finest level was the same from the work of Herrmann [17] which was given by $D/32$, where D is the jet exit diameter.

The two main characteristic dimensionless numbers related to JICF are the Reynolds and Weber numbers [14], as well as the momentum flux ratio [6]. According to Ingebo [28], the maximum droplet diameter depended on the Reynolds and Weber numbers [28]. In addition, the jet penetration as well as the breakup process itself is severely influenced by the Weber number [14]. Table 1 summarizes the operating conditions and the relevant characteristic dimensionless numbers.

A turbulent velocity profile was imposed to the jet inlet section in order to introduce turbulence effects at the liquid inlet section. In the work of Herrmann [17], the turbulence effects were introduced using instantaneous inlet velocity sections which were given by a previous simulation exclusively of a small region close to the inlet section and a small flow region before the jet inlet section. Ghods and Herrmann [29] reported a comparison between different inlet conditions and it was shown that the imposition of a turbulent velocity profile presented similar atomization results compared to the model including instantaneous velocity inlet sections. Therefore, the imposition of a turbulent analytical velocity profile in the inlet section was a reasonable approximation since Ghods and Herrmann [29] reported low influence of the inlet conditions to the liquid breakup process.

The mathematical equation employed to compute the turbulent velocity profile was given by the following expression:

$$V = V_{\max}\left(1 - \frac{r}{R}\right)^{1/5}, \tag{16}$$

where $V_{\max}$ is the maximum velocity which is 1.2 according to the theoretical solution available in White [18]. Figure 2

Table 1 Operating conditions and characteristic numbers

	Value	Unit
Jet exit diameter	0.0013	m
Crossflow specific mass	1.225	kg/m^3
Jet specific mass	12.25	kg/m^3
Crossflow velocity	120.4	m/s
Jet velocity	97.84	m/s
Crossflow viscosity	1.82×10^{-5}	kg/ms
Jet viscosity	1.11×10^{-4}	kg/ms
Surface tension coefficient	0.07	N/m
Momentum flux ratio	6.6	–
Crossflow Weber number	330	–
Jet Weber number	2178	–
Crossflow Reynolds number	5.7×10^5	–
Jet Reynolds number	1.4×10^4	–

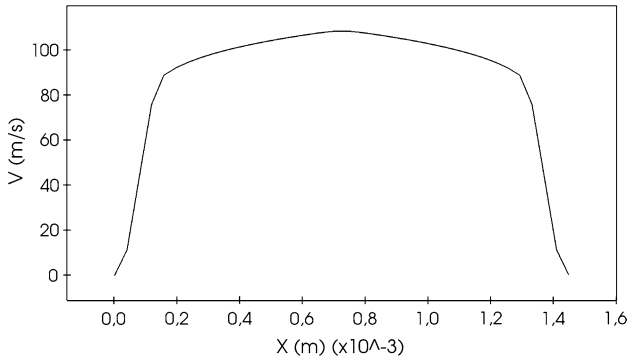

Fig. 2 Mean inlet flow velocity profile of the liquid jet from the present work according to the expression for the turbulent velocity profile previously reported

shows the inlet velocity profile of the turbulent jet from the present work.

The flow was at rest at the initial condition and considered isothermal during all the simulations, similarly to Herrmann [17]. The airflow was imposed as a uniform velocity field at the channel's inlet. According to the Reynolds number from the jet and the crossflow, shown in Table 1, the flow regime is definitely turbulent. The turbulence at the inlet of both simulations shares the same seed frequency. The numerical model was validated computing the spray penetration near the liquid injector as well as comparing the probability density function (pdf) of the droplets converted from the Eulerian to the Lagrangian approach with those of previous works.

3 Computational results

The case studied in the present paper was previously reported in Herrmann [17] and it consists of a turbulent liquid jet in crossflow. The liquid comes from a circular inlet section and is subjected to primary breakup process, where the liquid jet breaks up into several smaller structures, namely liquid sheets, ligaments and droplets [9]. As the jet emerges from the inlet, surface waves appear on the leeward side of the column, creating droplets from the leeward surface. The liquid column bents in the direction of the vapor flow breaking the liquid column into ligaments and finally into droplets due to aerodynamic forces [14].

3.1 General flow characteristics

The primary breakup consists of the moment when the liquid surface becomes unstable and ligaments are created. From these ligaments, droplets are created. After the primary breakup, it is generally believed that large droplets may break into smaller droplets and this process is called secondary breakup [5] which has not been studied in the present work.

As previously reported by Herrmann [17], the liquid jet emerges from the inlet section forming a liquid column which slightly deflects toward the crossflow direction. At the top of the liquid column in Fig. 3, it is evident the occurrence of the roll-up structures described by Herrmann [17]. Also at the top of the liquid column, it is possible to see some ligaments which are direct consequence of shear and will lead to rupture with multiple drops as seen in the toward the flow. Finally, behind the jet column it is observed some surface breakup structures composed by some drops and ligaments. The two main breakup mechanisms were observed in the simulation, namely surface and column breakup. Figure 3 shows a snapshot side view of the interface near the jet injector region using the standard VOF method.

One column breakup mode consisted of instability waves being generated and forming roll-up structures until the production of bag-like structures that break into multiple drops (shown in Fig. 3). According to Herrmann [17], the latter instability may be due to a Kelvin–Helmholtz instability, which was verified and confirmed by Grosshans et al. [8]. Another breakup mode observed is the generation of ligaments at the sides of the liquid jet near the injector which stretches out and then ruptures, forming a range of drop sizes. These ligaments are shown in Fig. 3 and eventually lead to multiple drops. Ligament formation is induced by local shear [5] and it was expected to observe these ligaments due to the high intensity of shear from the vapor crossflow. The presence of ligaments at the top of the liquid column is evident in Fig. 3. Here, the importance of the second criterion for the Euler–Lagrangian algorithm of conversion is illustrated, since the ligaments may respect the first criterion, but are not converted into Lagrangian points since they still need to be broken by primary mechanisms.

The surface breakup starts at the liquid inlet region; however, it is not limited to this region [30]. The column breakup is mainly governed by the propagation of waves growing on the jet surface until sufficiently amplified to cause the jet core to collapse [30]. According to the surface breakup observations from the simulations, ligaments are the main

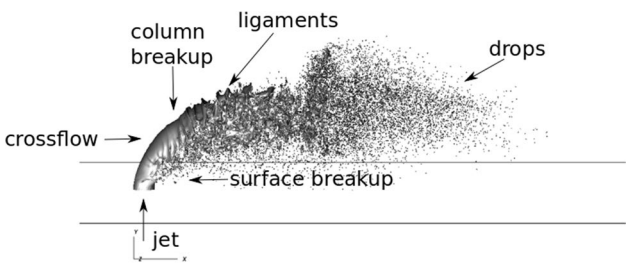

Fig. 3 Snapshot of the interface contour at time 0.00012 s of the simulation using the standard VOF method

liquid structures stripped from the sides of the liquid column. Regarding the velocity field, it is possible to identify the typical flow patterns from a von Karman vortex structure behind a bluff body [31], as previously found in the literature [30].

Figure 4 shows a snapshot of q-criterion contour from the simulation using the VOF method. A number of stretched turbulent structures are seen at the top of the liquid column, similarly located where the roll-up structures were previously seen with the interface contour. AMR provided a suitable mesh configuration to this problem since the fine grid covered most part of the turbulence structures as shown in Fig. 4.

A large number of ligaments seen at the top of the column present evidences of the roll-up structures previously described in Herrmann [17]. The presence of these ligaments from the q-criterion contour confirms the development of Kelvin–Helmholtz turbulent structures since the vorticity magnitude is greater than the strain effects.

At the start, we assume the flow in each layer is irrotational. However, there exists strong shear vorticity in the interface layer so the vorticity for the whole system does not equal zero. Kelvin–Helmholtz is basically a two-dimensional phenomenon; only later in its development, three-dimensional movements appear which leads to turbulent mixing. The large number of small structures from the q-criterion shown in Fig. 4 illustrates the high intensity of vorticity at the spray impact region where lots of surfaces are presented in different shapes and sizes. Figure 5 presents the interface contour (in gray) and the q-criterion contour (in black) at two different simulation times of the simulation using FGVT method.

According to Fig. 5, the q-criterion ligaments previously shown in Fig. 4 fit exactly where the interface present the roll-up structures.

Figure 5 presents the interface contour (in gray) and the q-criterion contour (in black) at two different simulation times of the simulation using FGVT method.

According to Fig. 6, the q-criterion ligaments are clearly close to the bag-like structures previously reported by the literature and it confirmed the rotational characteristic of these structures since q-criterion necessarily pointed out the rotational effects over the strain rate and it ratifies the occurrence of Kelvin–Helmholtz instabilities.

3.2 Comparison between VOF and FGVT

Although the liquid jet is in the turbulent regime and there are multiple nonlinear processes taking place at the cross-flow, after some simulation time, the liquid column position

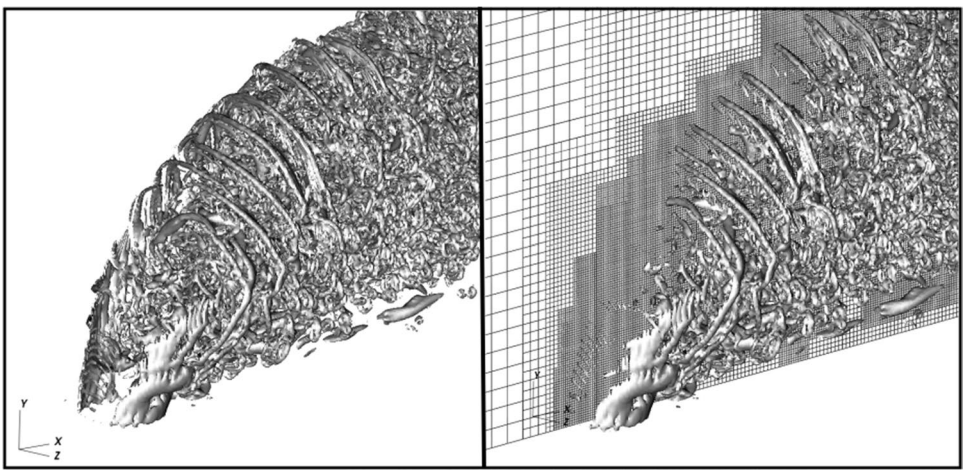

Fig. 4 Snapshot of q-criterion contour (left) and q-criterion contour with mesh configuration (right) at time 0.00009 s

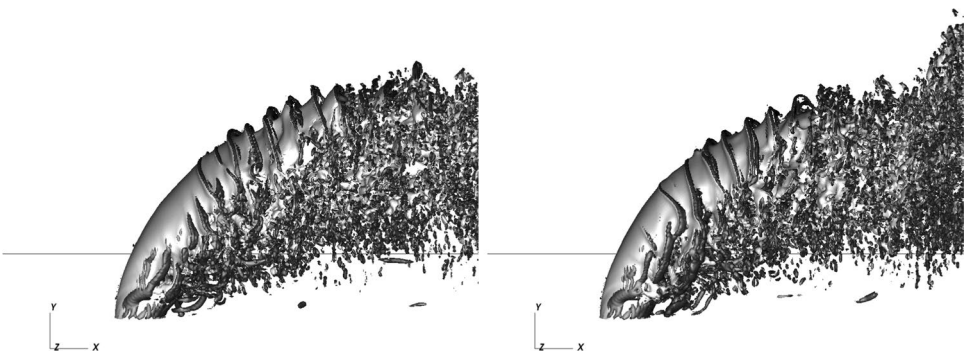

Fig. 5 Snapshot of interface contour (in gray) and the q-criterion contour (in black) at two different times from the simulation using FGVT method

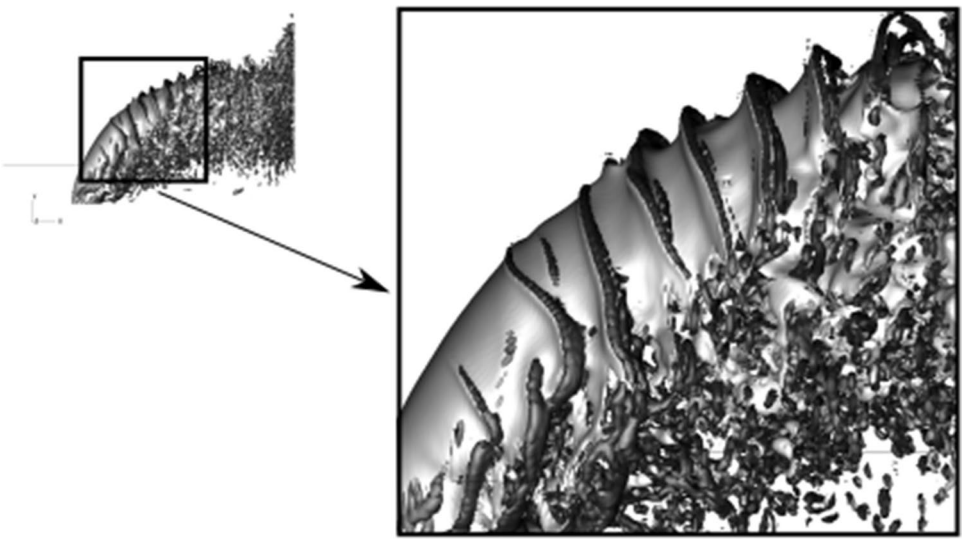

Fig. 6 Snapshot of interface contour (in gray) and the q-criterion contour (in black) and detail from the simulation using FGVT method

and the ligaments and droplet formation assumed a permanent pattern. Therefore, the validation with literature works was performed at the simulation time 0.000217 s, when the liquid column was completely formed and the breakup modes were well defined and interface contour presented a repeated pattern in time.

Spray penetration is defined as the maximum transverse distance reached by these droplets [14]. It is known that spray penetration depends on the trajectory of the liquid column near the injector. The trajectory of the liquid column establishes the initial location of droplets as they detach from the liquid jet. In addition, bending of the liquid column in the direction of vapor reduces the linear momentum of both the jet and the resulting droplets. Finally, the reduced linear momentum diminishes the spray penetration downstream of the injector [14].

The jet penetration was compared with predictions of two common correlations for the penetration of the emerging liquid jet derived by fitting experimental data, namely the correlations from Wu et al. [32] and Stenzler et al. [14].

The correlation from Wu et al. [32] is given by the following expression:

$$\frac{y}{D} = 1.37\left(q\frac{x}{D}\right)^{(1/2)}. \tag{17}$$

On the other hand, the correlation from Stenzler et al. [14] is given by the following equation:

$$\frac{y}{D} = 2.63q^{0.442}\left(\frac{x}{D}\right)^{0.39} We^{-0.088}\left(\frac{\mu_l}{\mu_{H_2O}}\right)^{-0.027}. \tag{18}$$

Herrmann [17] reported a better agreement with the latter correlation compared to the correlation from Wu et al. [32]. Both correlations are valid only in the near-injector region. Figure 7 shows the results of the jet penetration from the present work in comparison with the correlations of Wu et al. [32] and Stenzler et al. [14].

According to Fig. 7, a good agreement between the results from the present paper and the experimental correlations from the literature was obtained. As previously found by Herrmann [17], the correlation from Stenzler et al. [14] presented lower deviation to the data obtained compared to the correlation from Wu et al. [32]. According to the results found for jet penetration, both methods provided identical

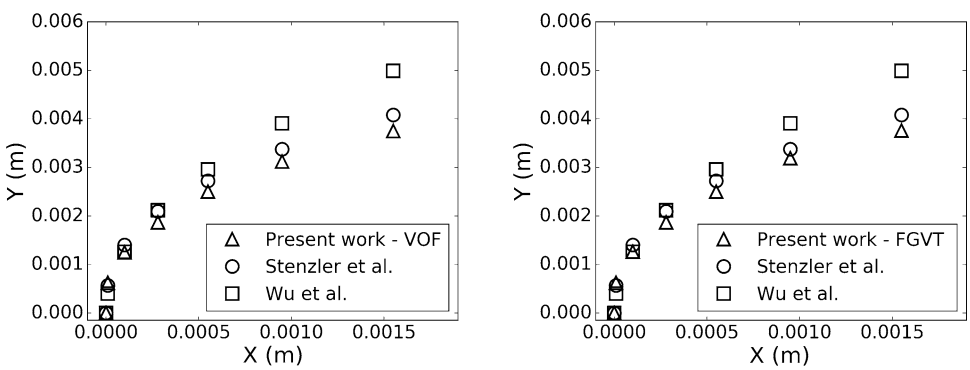

Fig. 7 Jet penetration compared with the correlations of Wu et al. [32] and Stenzler et al. [14]

results; then, for jet penetration analysis, FGVT method does not show any advantage compared to the VOF method. In fact, Herrmann [17] reported a low influence of mesh quality in this comparison.

The dimensionless probability density function (pdf) was computed in order to compare the data found in the simulations from the present work with the simulation previously performed by Herrmann [17]. Only the Lagrangian drops were computed which were tracked using the point particle description after the conversion from the Eulerian approach. No secondary breakup model was employed; therefore, the droplet diameter remains constant in time after the conversion to the Lagrangian approach. The drop size distribution using the pdf were generated by binning the date into 20 bins of equal size in terms of D, which is the jet inlet diameter. The approximate total number of droplets used was 40,000, as previously found by Herrmann [17]. The pdf was normalized by a factor of 0.0078.

Figure 8 shows a comparison between the dimensionless probability density function (pdf) found using VOF and using FGVT method. According to Fig. 8, the simulation using VOF provided relatively less small drops compared to FGVT. The grid resolution severely impacted on the small drops representation as previously reported by Herrmann [17] and Grosshans et al. [8]. Since the FGVT method was able to advect the interface using a finer grid than VOF, the pdf accuracy for the small droplets was good compared to the pdf from VOF. Probably, some detailed interface resolution was relevant to some breakup processes, and then, small droplet formation shown in Fig. 8 is in higher number only with FGVT.

Besides the jet penetration and the breakup modes, relevant information to engineering applications related to JICF is the drop size distribution obtained in the computational simulations. According to Movaghar et al. [3], drop size distribution is one of the main outputs of the primary breakup simulations. Figure 9 shows the histograms of the drop size distribution from the computational data obtained with the VOF (left) and FGVT (right) methods.

According to Fig. 9, most part of the drop size was approximately 0.00005 m which was the same order of magnitude found previously by Herrmann [17]. This size was equivalent to close to one-hundredth of the jet exit diameter. The FGVT method was able to provide droplets smaller than 0.00005 m; however, the smallest droplets found using VOF were approximately 0.00005 m.

The breakup process was severely affected by the mesh resolution used in the computational simulations, as previously reported by Herrmann [17]. In course grids, small-scale turbulent eddies do not initiate atomization; on the other hand, grids with high resolution do resolve more small turbulent scales which may corrugate the interface and therefore initiate atomization. Therefore, it was expected to obtain a higher number of droplets in FGVT method in

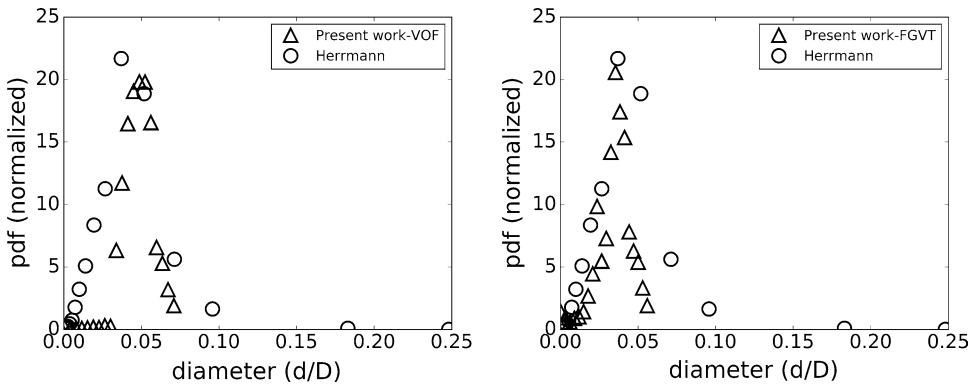

Fig. 8 Comparison between drop size distribution using VOF (left) and FGVT (right) methods with Herrmann [17], according to the pdf

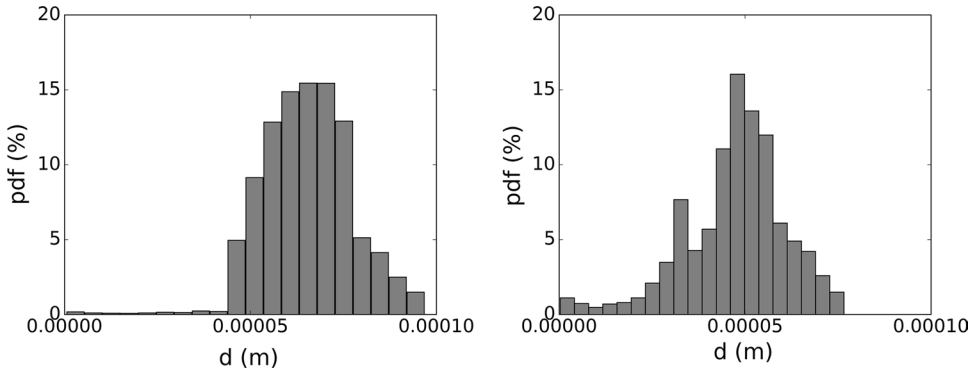

Fig. 9 Drop size distribution according to histograms from the computational results obtained for VOF (left) and FGVT (right) methods at time 0.0006 s

comparison with VOF, as well as a higher number of droplets with smaller size compared to VOF.

A comparison between the interface contour between the simulations using VOF and FGVT methods is shown in Fig. 10.

According to Fig. 10, the number of droplets seen in the simulation with FGVT was deeply higher than the simulation with VOF. In addition, the interface details seen in the simulation with FGVT were captured more precisely as some ligaments and drops were better identified. Finally, the column and surface breakup modes seen with FGVT method were more evident and severe compared to the VOF method.

The number of droplets converted into the Lagrangian approach was significantly improved by the use of the FGVT method compared to the VOF method itself, as shown in Fig. 11.

Therefore, as shown in Fig. 11, the FGVT method allowed a higher resolution of interface which improved the number of Eulerian droplets ready to be converted to the Lagrangian approach.

In order to run the simulation using FGVT, it was required to reduce the time step by half; otherwise, the numerical methods presented convergence difficulties. In addition, the simulation velocity using the FGVT method was lower than the simulation using VOF. Considering different simulation moments, the time step using VOF was approximately 14% faster than the time step using FGVT. The time step from FGVT is computationally more expensive due to the interface advection in a finer grid as well as the more numerical challenging discontinuities of fluid properties and variables.

The AMR technique reduced significantly the number of cells required to run the simulations with high accuracy and moderate computational costs. As shown in Fig. 12, away from the interface region, a course grid is used to solve most part of the computational domain.

The AMR technique reduced the required number of cell in approximately three orders of magnitude compared to a uniform grid. In Fig. 12, it is possible to see in detail the refined mesh only close to the interface region. Therefore, AMR is an option to conduct three-dimensional primary breakup simulations, as previously found by Shinjo et al. [5]. The high resolution close to the interfacial region shown in

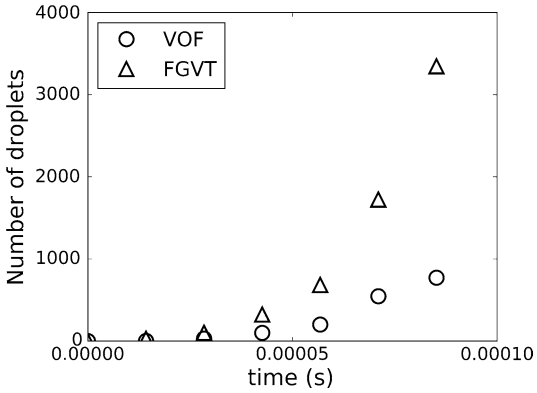

Fig. 11 Number of droplets converted from the Eulerian to the Lagrangian approach using VOF and FGVT methods

Fig. 12 allows the representation of the interface with high fidelity compared to the courser grids away from the interface. The high mesh resolution is confirmed by the visualization of even Kelvin–Helmholtz instabilities at the top of the liquid column in Fig. 12.

4 Conclusions

The VOF and the FGVT methods were tested to a liquid jet in crossflow in order to verify the potential of FGVT method to provide a higher interface accuracy, thereby improving quality of breakup effect to the simulations. The VOF and the FGVT methods performance were evaluated, and FGVT method provided higher accuracy compared to the VOF method. The model was validated according to the jet trajectory and droplet size distribution with low differences from the literature. Two main breakup modes were identified, namely the column and surface breakup as the literature previously reported.

The FGVT method presented a better interface representation from the VOF and its difference affected the Eulerian–Lagrangian conversion, by increasing significantly the number of droplets converted. Severely more smaller droplets were captured with FGVT approach compared to VOF, and the details about the interface contour were particularly

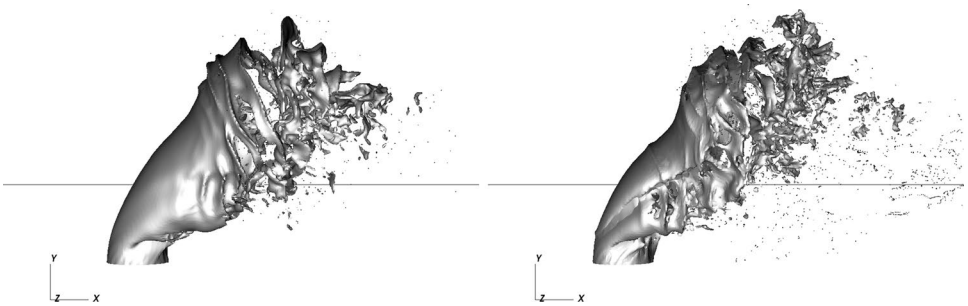

Fig. 10 Interface contour at time 0.000071 s of the simulation using the VOF method (left) and the FGVT method (right)

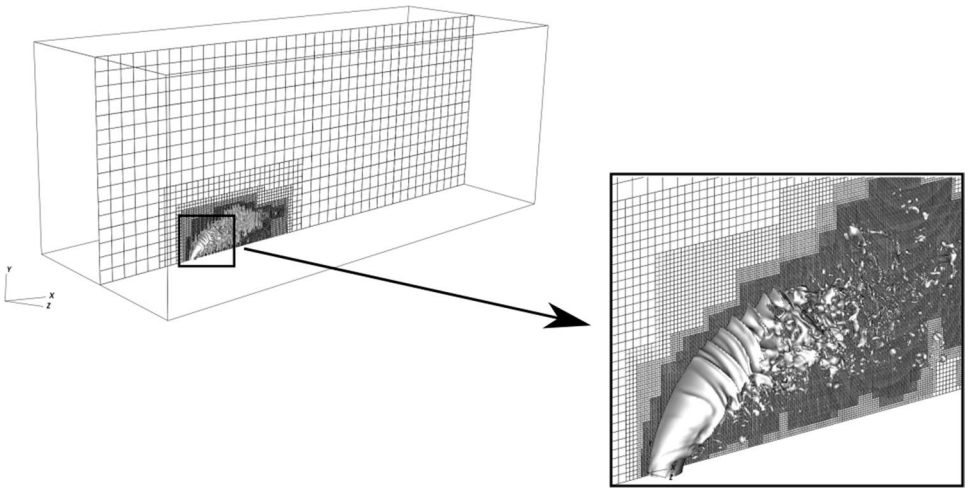

Fig. 12 Interface contour and mesh configuration at time 0.00006 s of the simulation using the VOF method

better described using FGVT instead of VOF. The FGVT simulation was slower compared to VOF simulation since it required a lower time step.

Kelvin–Helmholtz instabilities were identified and a number of turbulent coherent structures typically present in JICF. The location of multiple ligaments from q–criterion confirmed the occurrence of Kelvin–Helmholtz instabilities at the top of the jet liquid column, specially at the interface regions known as bag-like structures and roll-ups.

Large computational costs were spared using AMR, because of the considerable reduction in the number of computational cells required. In addition, the refinement criterion of interface presence was considered adequate to perform all the simulations, providing results with good resolution and smaller computational costs compared to simulations using uniform grids.

Acknowledgements The authors gratefully acknowledge financial support from Petrobras, CNPQ, Fapemig and Capes. The authors are also grateful to the mechanical engineering graduate program from the Federal University of Uberlândia (UFU).

References

1. Hirt CW, Nichols BD (1981) Volume of fluid (VOF) method for the dynamics of free boundaries. J Comput Phys 39:201. https://doi.org/10.1016/0021-9991(81)90145-5
2. Rudman M (1998) A volume-tracking method for incompressible multifluid flows with large density variations. Int J Numer Methods Fluids 28:357. https://doi.org/10.1002/(SICI)1097-0363(19980815)28:2<357:AID-FLD750>3.0.CO;2-D
3. Movaghar A, Linne M, Herrmann M, Kerstein A, Oevermann M (2018) Modeling and numerical study of primary breakup under diesel conditions. Int J Multiph Flow 98:110. https://doi.org/10.1016/j.ijmultiphaseflow.2017.09.002
4. Jain M, John B, Iyer K, Prabhu S (2014) Characterization of the full cone pressure swirl spray nozzles for the nuclear reactor containment spray system. Nucl Eng Des 273:131. https://doi.org/10.1016/j.nucengdes.2014.02.025
5. Shinjo J, Umemura A (2010) Simulation of liquid jet primary breakup: dynamics of ligament and droplet formation. Int J Multiph Flow 36:513. https://doi.org/10.1016/j.ijmultiphaseflow.2010.03.008
6. Xiao F, Dianat M, McGuirk J (2014) LES of turbulent liquid jet primary breakup in turbulent coaxial air flow. Int J Multiph Flow 60:103. https://doi.org/10.1016/j.ijmultiphaseflow.2013.11.013
7. Bravo L, Kim D, Ham F, Kerner K (2018) In: Conference: 2018 joint propulsion conference, pp 1–12. https://doi.org/10.2514/6.2018-4683
8. Grosshans H, Movaghar A, Cao L, Oevermann M, Szsz RZ, Fuchs L (2016) Sensitivity of VOF simulations of the liquid jet breakup to physical and numerical parameters. Comput Fluids 136:312. https://doi.org/10.1016/j.compfluid.2016.06.018
9. Turner M, Sazhin S, Healey J, Crua C, Martynov S (2012) A breakup model for transient diesel fuel sprays. Fuel 97:288. https://doi.org/10.1016/j.fuel.2012.01.076
10. Bravo L, Kim D, Ham F, Su S (2018) Computational study of atomization and fuel drop size distributions in high-speed primary breakup. At Sprays 28:321. https://doi.org/10.1615/AtomizSpr.2018018917
11. Denner F, van der Heul DR, Oud GT, Villar MM, Silveira-Neto A, van Wachem BG (2014) Comparative study of mass-conserving interface capturing frameworks for two-phase flows with surface tension. Int J Multiph Flow 61:37. https://doi.org/10.1016/j.ijmultiphaseflow.2013.12.011
12. Duarte BAF, Serfaty R, Silveira-Neto A (2019) Direct contact condensation jet in cross-flow using computational fluid dynamics. J Heat Transf 141:55. https://doi.org/10.1115/1.4042779
13. Lee MS, Aute ARV (2017) Direct numerical simulation of incompressible multiphase flow with phase change. J Comput Phys 344:381. https://doi.org/10.1016/j.jcp.2017.04.073
14. Stenzler JN, Lee JG, Santavicca DA, Lee W (2006) Penetration of liquid jets in a cross-flow. At Sprays. https://doi.org/10.1615/AtomizSpr.v16.i8.30
15. Li X, Soteriou M (2018) Detailed numerical simulation of liquid jet atomization in crossflow of increasing density. Int J Multiph Flow 104:214. https://doi.org/10.1016/j.ijmultiphaseflow.2018.02.016
16. Duarte BAF, Villar MM, Serfaty R, Silveira-Neto A, Braz J (2019) Evaluation of a diffuse interface treatment for pressure

in phase change simulations using adaptive mesh refinement. Soc Mech Sci Eng 41:575. https://doi.org/10.1007/s40430-019-1580-7
17. Herrmann M (2010) Detailed numerical simulations of the primary atomization of a turbulent liquid jet in crossflow. J Eng Gas Turbines Power 132:506. https://doi.org/10.1115/1.4000148
18. White FM, Corfield I (2006) Viscous fluid flow. McGraw-Hill, New York
19. Jeong J, Hussain F (1995) On the identification of a vortex. J Fluid Mech 285:69. https://doi.org/10.1017/S0022112095000462
20. Wachem BGM, Schouten JC (2002) Experimental validation of 3-D Lagrangian VOF model: bubble shape and rise velocity. AIChE J 48:253. https://doi.org/10.1002/aic.690481205
21. Brackbill JU, Kothe DB, Zemach C (1992) A continuum method for modeling surface tension. J Comput Phys 100:335. https://doi.org/10.1016/0021-9991(92)90240-Y
22. Chorin AJ (1968) Numerical solution of the Navier–Stokes equations. Math Comput 22:745. https://doi.org/10.1090/s0025-5718-1968-0242392-2
23. Centrella JM, Wilson JR (1984) Planar numerical cosmology. II—The difference equations and numerical tests. Astrophys J Suppl Ser 54:229. https://doi.org/10.1086/190927
24. Duarte BAF, Serfaty R, Silveira-Neto A (2019) Influence of the Prandtl number on wall-to-fluid thermal transfer rate in a cubic cavity. Flow Turbul Combust 142:1. https://doi.org/10.1007/s10494-019-00025-z
25. Akhtar M, Kleis S (2013) Boiling flow simulations on adaptive octree grids. Int J Multiph Flow 53:88. https://doi.org/10.1016/j.ijmultiphaseflow.2013.01.008
26. Deen N, Kuipers J (2013) Direct numerical simulation of wall-to liquid heat transfer in dispersed gas–liquid two-phase flow using a volume of fluid approach. Chem Eng Sci 102:268. https://doi.org/10.1016/j.ces.2013.08.025
27. Barbi F, Pivello MR, Villar MM, Serfaty R, Roma AM, Silveira-Neto A (2018) Numerical experiments of ascending bubbles for fluid dynamic force calculations. J Braz Soc Mech Sci Eng 40:519. https://doi.org/10.1007/s40430-018-1435-7
28. Ingebo RD (1967) NASA Report TM X-1363
29. Ghods S, Herrmann M (2013) In: International conference on multiphase flow, vol 132, p 50. https://doi.org/10.1115/1.4000148
30. Behzada M, Ashgriz N, Karneya BW (2016) Surface breakup of a non-turbulent liquid jet injected into a high pressure gaseous crossflow. Int J Multiph Flow 80:100. https://doi.org/10.1016/j.ijmultiphaseflow.2015.11.007
31. Li X, Soteriou M (2016) High fidelity simulation and analysis of liquid jet atomization in a gaseous crossflow at intermediate Weber numbers. Phys Fluids 28:1. https://doi.org/10.1063/1.4959290
32. Wu P, Fuller RP, Kirkendall KA, Nejad AS (1997) Breakup processes of liquid jets in subsonic crossflows. J Propul Power 13:64. https://doi.org/10.2514/2.5151